


## Electrical Control of Ultrafast Magnetic Speeds in Graphene Spin Field-Effect Junctions

David Muradas-Belinchón<sup>1,\*</sup>, Suchetana Mukhopadhyay<sup>1,2,3,\*</sup>, Francesco Foggetti<sup>1</sup>, Surya N. Panda,<sup>2</sup> Olof Karis<sup>1</sup>, Peter M. Oppeneer<sup>1</sup>, Anjan Barman<sup>1,2,†</sup> and M. Venkata Kamalakar<sup>1,‡</sup>

<sup>1</sup>*Department of Physics and Astronomy, Uppsala University, Box 516, Uppsala SE-751 20, Sweden*

<sup>2</sup>*Department of Condensed Matter and Materials Physics, S. N. Bose National Center for Basic Sciences, Block JD, Sector III, Salt Lake, Kolkata 700106, India*

<sup>3</sup>*Department of Physical Sciences, Indian Institute of Science Education and Research Kolkata, Mohanpur, West Bengal 741246, India*

 (Received 28 January 2025; revised 27 April 2025; accepted 25 July 2025; published 28 August 2025)

We demonstrate ultrafast graphene spin-field-effect junctions, where gate-tunable superdiffusive spin currents across graphene-ferromagnet interfaces enable electric field control of magnetization dynamics in the ferromagnet. By electrostatically tuning the Fermi level in graphene underlying a cobalt thin film, we modulate the ultrafast spin transport across graphene-cobalt interfaces, reducing femtosecond laser-induced demagnetization time from 203 fs in bare cobalt thin films to 93 fs, a more than 100% increase in the rate of magnetization quenching. Supported by superdiffusive spin transport calculations, our findings unlock field-tunable magnetic speeds in devices, paving the way for innovations in subpicosecond spintronic memory-logic operations. Furthermore, this work creates new possibilities for electrical modulation of spin dynamics and ultrafast spin injection into two-dimensional quantum materials, with potential for next-generation quantum sensors and faster magnetic technologies.

DOI: [10.1103/7ldk-csp9](https://doi.org/10.1103/7ldk-csp9)

Harnessing spin currents in magnetic tunnel junctions has driven spintronic inventions of nonvolatile, high-density memory storage, precision magnetoresistive sensors, and energy-efficient magnetic random-access memories. Beyond these existing technologies, realizing electrical manipulation of ultrafast magnetic phenomena can pave the way for energy-efficient, fast spin-logic integrated circuits [1], neuromorphic devices [2], precision quantum sensors [3], and terahertz technologies [4]. Conventionally, femtosecond magnetization dynamics in metallic multilayers [5,6] has been attributed to superdiffusive spin transport across ferromagnet (FM)-nonmagnet (NM) metallic junctions [7]. However, due to the screening effect and low spin diffusion lengths in metals, the electric field manipulation of ultrafast spin transport in metallic junctions is not feasible. Although semiconductors offer electric field tunability of interfaces, conductivity mismatch [8] and low spin diffusion limit junctions involving semiconductors, and realizing precise modulation of ultrafast spin currents remains a challenge. Here, electrically tunable

two-dimensional (2D) materials like graphene offer distinct functionality in proximity to magnets [9]. Graphene's linear dispersion and massless fermions enable high carrier mobility and ballistic transport [10,11], which along with its intrinsically low spin relaxation [12], make it ideal for spin transport [13–15] and spin-dependent junctions [9]. The field-tunable carrier density provides a unique means to control spin currents in graphene-ferromagnet heterostructures, toward advancing high-speed graphene spintronic applications.

In this Letter, we demonstrate graphene spin-field-effect junctions (GSFEJs), where the electric field can control ultrafast spin currents and spin dynamics in thin-film ferromagnets. We combine electrical measurements and all-optical time-resolved magneto-optical Kerr effect (TR-MOKE) probes to measure rapid demagnetization in the FM contacts while tuning the carrier concentration in graphene. Our experiments employing direct contacts as well as contacts involving tunnel barriers show efficient gate control, with over 100% enhancement in the demagnetization rate (magnetization quenching speed) compared to bare Co by modulating the junction resistance. Superdiffusive spin transport calculations validating our experimental results establish a new mechanism of field-enhanced magnetization dynamics in a device without structural or material modifications. Our findings represent a major step toward low-power, faster spintronic devices for memory-logic applications and emerging quantum technologies.

\*These authors contributed equally to this work.

†Contact author: [abarman@bose.res.in](mailto:abarman@bose.res.in)

‡Contact author: [venkata.mutta@physics.uu.se](mailto:venkata.mutta@physics.uu.se)

*Published by the American Physical Society under the terms of the [Creative Commons Attribution 4.0 International license](https://creativecommons.org/licenses/by/4.0/). Further distribution of this work must maintain attribution to the author(s) and the published article's title, journal citation, and DOI. Funded by [Bibsam](https://www.bibsam.org/).*

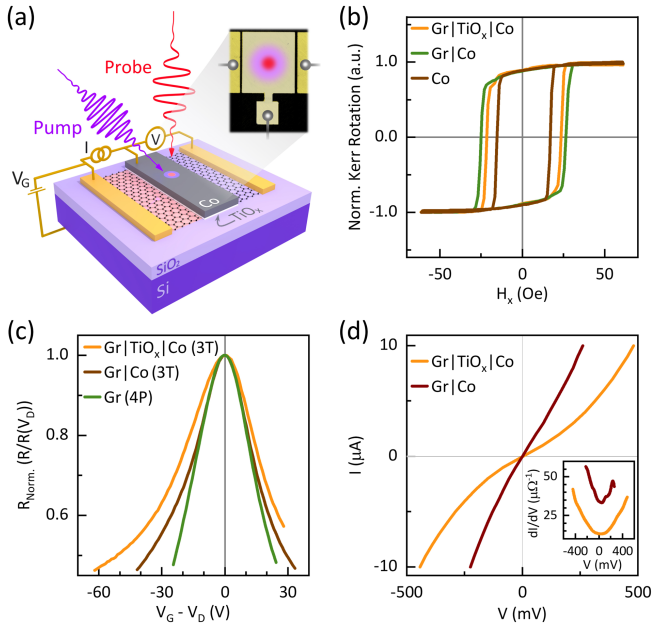


FIG. 1. Device scheme and static characterization. (a) Experimental setup for spin dynamics measurements in GSFEJs, featuring a CVD graphene channel and ferromagnetic contacts, with a fabricated device and pump-probe spots indicated in the inset. (b) Static MOKE magnetization curves for Gr|Co, Gr|TiO<sub>x</sub>|Co, and bare Co with 30 nm thick Co. (c) Gate-voltage-dependent normalized resistance (relative to the resistance at the Dirac point voltage  $V_D$ ) for Gr|TiO<sub>x</sub>|Co and Gr|Co junctions measured in three-terminal (3T) configuration, and for the graphene channel measured in four-probe (4P) configuration. (d)  $I$ - $V$  and differential conductance  $dI/dV$  (inset) of Gr|TiO<sub>x</sub>|Co and Gr|Co devices, showing tunneling behavior.

In Fig. 1(a), we show a schematic of the GSFEJ devices, illustrating graphene overlaid with FM contacts (Gr|FM) and a bottom gate electrode integrated with a TR-MOKE pump-probe setup. The gate voltage tunable carrier concentration in graphene modulates the Gr|FM junction resistance ( $R_J$ ), controlling superdiffusive spin currents and the ensuing FM demagnetization. The GSFEJs were fabricated [Supplemental Material (SM) [16]] with chemical vapor deposited (CVD) graphene and ferromagnetic contacts (with and without TiO<sub>x</sub> tunnel barriers) with thicknesses of the order of the typical spin diffusion length ( $\lambda_s$ ) and mean free path ( $\lambda_p$ ) in Co [23] to facilitate nearly ballistic spin transport across junctions. When an ultrashort laser pulse is incident on the FM, it excites nonthermal hot electrons. These electrons, with different spin-dependent scattering rates for up ( $\uparrow$ ) and down ( $\downarrow$ ) spin ( $\sigma_\uparrow > \sigma_\downarrow$ , with  $\sigma$  the spin-dependent conductivity), generate spin currents that superdiffuse into adjacent materials (graphene), instantly quenching the magnetism in the FM layer. Since the magnetic moment is transferred by the spin-polarized electrons injected from the FM layer to the underlying graphene layer in GSFEJs, the ultrafast spin dynamics in the FM are expected to depend on the Gr|FM

interface conductivity, which we modulate here via an applied gate voltage ( $V_G$ ). Typically, interfaces extend over  $\sim 1$  nm, across which the electronic chemical potentials of the metal and graphene equilibrate.

To characterize the Gr|FM heterostructures in GSFEJ devices, we measured the magnetic behavior of the as-deposited Co heterostructures using a static nanoMOKE system. Figure 1(b) presents the magnetization curves at room temperature for 30 nm Co in Gr|Co, Gr|TiO<sub>x</sub>|Co, and Co heterostructures, showing coercivities of 25.7, 22.5, and 16.1 Oe, respectively. Compared to bare Co, the enhanced coercivity in the heterostructures with graphene can be linked to greater domain pinning centers [17]. All samples revealed magnetic uniformity throughout the patterned magnetic contact structures (Fig. S1 in SM shows the mapping of different sample thicknesses with and without graphene, as well as with and without a tunnel barrier [16]). We performed gate-voltage-dependent charge transport measurements on the devices to assess the electrical quality of the channel and interfaces (Fig. S2 in SM shows carrier density  $n$  tuning with  $V_G$  [16]). In Fig. 1(c), we display the gate-dependent Dirac curves obtained by three-terminal measurements (contacts) and four-probe measurements (channel) [13]. Despite a shift in charge neutrality points ( $V_D$ ) due to surface charge transfer doping [13,24], sharp Dirac curves for Gr|Co contacts, similar to the graphene channel, indicate an unaltered band structure of graphene, maintaining the electron-hole symmetry and carrier mobility of  $\sim 2000$  cm<sup>2</sup> V<sup>-1</sup> s<sup>-1</sup>. Graphene exhibiting such electrical quality shows high diffusive [25] and long-distance spin transport [13,26]. In addition, as shown in Fig. 1(d), the current-voltage ( $I$ - $V$ ) characteristics and the differential conductance ( $dI/dV$ ) plot for junctions with TiO<sub>x</sub> show pronounced tunneling behavior. The introduction of TiO<sub>x</sub> is known to improve spin injection into graphene [13], circumventing the conductivity mismatch issue [8]. These measurements confirm the magnetic nature and electrical tunability in Gr|(TiO<sub>x</sub>)Co junctions.

Having assessed the magnetic properties and electrical control in GSFEJs, we probed the ultrafast spin dynamics in the junctions. As depicted in Fig. 1(a), we employ all-optical TR-MOKE magnetometry using a two-color optical pump-probe technique [18] to perform spin dynamics measurements on all samples (further described in SM along with Fig. S3 [16]). Different heterostructure configurations of Gr|(TiO<sub>x</sub>)Co junctions, with and without TiO<sub>x</sub> (0.8 nm), with and without graphene, and varying Co thicknesses (10, 20, and 30 nm) allow for a wide range of conditions under which Gr|FM interface-controlled superdiffusive spin transport can be investigated and compared. Figure 2(a) shows the distinct demagnetization curves of 30 nm Co layers, obtained on four different samples viz., Co, TiO<sub>x</sub>|Co, Gr|Co, and Gr|TiO<sub>x</sub>|Co (see Fig. S4 in SM for 10 and 20 nm Co layers [16]). We quantify the observed spin dynamics with demagnetization ( $\tau_m$ ) and fast remagnetization ( $\tau_e$ ) times using the phenomenological

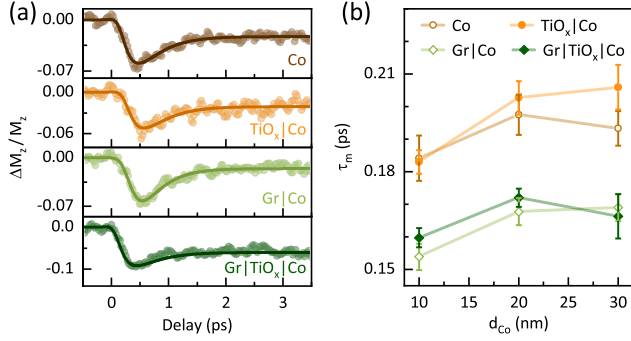


FIG. 2. Ultrafast demagnetization in Gr|FM heterostructures. (a) TR-MOKE curves showing demagnetization and recovery dynamics of 30 nm thick Co in different heterostructure configurations, with solid lines representing fits using Eq. (A1). (b)  $\tau_m$  versus Co thickness on four different heterostructures (for visualization purposes, the error bars are divided by 3).

three-temperature thermodynamic model (described in Appendix A).

Figure 2(b) shows the  $\tau_m$  of the four different heterostructures, all with varying Co thicknesses of 10–30 nm. The extracted values of  $\tau_m$  and  $\tau_e$  for various heterostructures are listed in Table S1 in SM [16]. Figure 2(b) shows similar  $\tau_m$  for Co and Co on TiO<sub>x</sub>. This similarity arises because the thin layer of TiO<sub>x</sub>, as a band insulator, is not expected to have much of an impact on the demagnetization process. However, when the Co is evaporated on top of graphene, the  $\tau_m$  is reduced by 12.6%–16.4% compared to the bare Co thin films, confirming spin current across Gr|FM heterostructures [7]. Similarly, in heterostructures containing an ultrathin (0.8 nm) TiO<sub>x</sub> barrier between the graphene and the Co, we observe a reduction between 12.7% and 19.3% compared to the bare Co thin films. Across all samples, thicker Co thin films exhibit longer  $\tau_m$ , likely due to slower hot electron scattering at the boundary or longer time spent by the electrons within the Co thin film. Overall, within the estimation error of all these samples, the presence of graphene decreases  $\tau_m$  by 15% due to the superdiffusive spin transport across the Gr|FM interface. Note that 0.8 nm TiO<sub>x</sub> is an optimal tunnel barrier width employed for efficient spin-polarized tunneling in graphene spintronic devices [13]. Therefore, for hot electron transport, the ultrathin TiO<sub>x</sub> barrier is expected to exhibit a similar transparency as direct Co on graphene and, accordingly, a similar reduction of  $\tau_m$  in samples with and without tunnel barriers. In contrast to the decrease in  $\tau_m$ , the extracted remagnetization times obtained from fitting remain largely unaltered with  $\tau_e \sim 350$  fs for all the samples [Fig. S4(c) in SM [16]]. Since remagnetization is a slower process linked to the electron-lattice interaction and subsequent heat dissipation out of the magnetic thin film, the effect of the heterostructure on  $\tau_e$  is relatively minor.

The proximity of a nonmagnetic conducting medium, such as graphene or copper, can accelerate magnetization quenching in NM|FM heterostructures. Here, varying the heterostructure composition allows further control of  $R_J$  and  $\tau_m$ , as displayed in Fig. 2(b), showing a sizeable variation of the  $\tau_m$  with interface media. To advance further, exploring the tunability of interface conductance ( $G_J = 1/R_J$ ) is critical for electrical control of spin dynamics, where Gr|FM heterostructures with and without tunnel barriers can be harnessed, as the adjacent graphene layer, offers tunability of spin current transmission. Since graphene is a semimetal with a linear energy-momentum dispersion and a high spin diffusion coefficient, it can conduct spin currents thousands of times longer than ordinary metals [13]. Moreover, by applying a gate voltage, the carrier concentration can be effectively tuned to alter  $R_J$ . As shown in Fig. 1(c), the gate serves as a reliable means to tune  $R_J$  by a factor of 2 or more by electrostatically tuning the Fermi level, which presents the potential for significant engineering in the spin dynamics of the overlying Co thin film. Enabling high electrical control of graphene is key here, and by optimized fabrication, we have obtained such tunability for graphene under Co, both with and without a tunnel barrier. To uncover field-effect spin dynamics in GSFEJs, we performed TR-MOKE measurements under various gate voltages ( $V_G$ ) relative to the Dirac point ( $V_D$ ), enabling Fermi-level tuning across both electron and hole conduction regimes. Figure 3(a) presents gate-voltage-dependent TR-MOKE traces measured on the Gr|TiO<sub>x</sub>|Co (30 nm) junctions (full datasets for 10, 20, and 30 nm junctions are provided in Fig. S5 in SM [16]). Distinct demagnetization curves are observed for different gate voltages ( $\Delta V = V_G - V_D$ ). The extracted  $\tau_m$  as a function of the  $\Delta V$  shown in Fig. 3(b), demonstrates that  $\tau_m$  in Co can be tuned by gate voltage in GSFEJs. Notably, Fig. 3(b) shows a clear peak at the Dirac point for all the samples. In Fig. 3(c), we compare the fastest demagnetization rates ( $\sim 1/\tau_m$ ) for each heterostructure in GSFEJs with those of TiO<sub>x</sub>|Co junctions. Since the laser absorption is expected to be more efficient in thicker films, the thicker junctions exhibit enhanced and reliable field tunability in  $\tau_m$ . To understand the junction conductance-dependent demagnetization times, we measured  $R_J$  in the three-terminal configuration [shown in Fig. 1(a)] while the magnetization dynamics were acquired. In Fig. 3(d), we show a striking dependence of  $\tau_m$  on the  $G_J$  of each sample, normalized to its maximum value for each junction, with the horizontal error bars representing the spread in  $G_J$ , primarily arising from laser-induced drift. These plots show a slower  $\tau_m$  in the same samples when the contact resistance is maximized, with the maximum  $\tau_m$  observed at  $V_D$ . As gate voltages reduce the  $R_J$ , we observe faster magnetization quenching, with the effect being more pronounced for voltages farther away from the Dirac point, where maximum electron or hole doping is achieved in graphene.

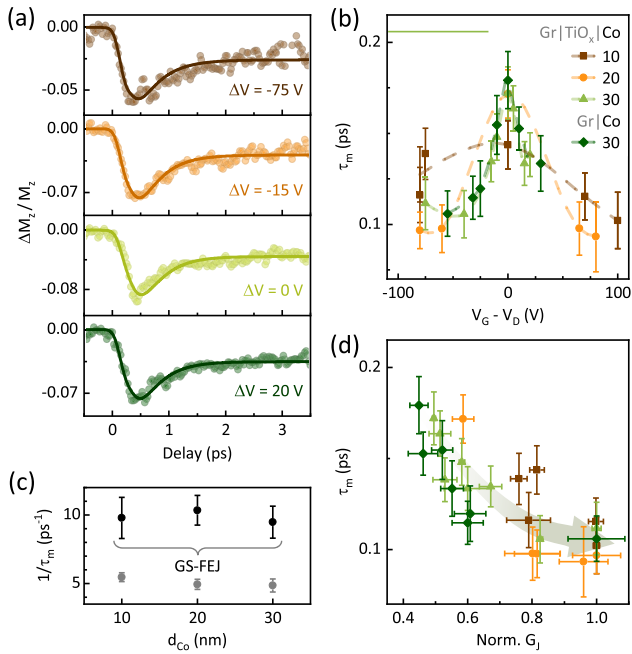


FIG. 3. Gate-tunable ultrafast spin dynamics in graphene spin-field-effect junctions. (a) TR-MOKE curves for Gr|TiO<sub>x</sub>|Co (30 nm) at gate voltages ( $V_G$ ) around the Dirac point ( $V_D$ ) with solid lines representing fits using Eq. (A1). (b)  $\tau_m$  versus gate voltage for four heterostructures. The green reference line represents  $\tau_m$  for bare TiO<sub>x</sub>|Co (30 nm). Dashed lines are guides to the eye. (c) Maximum demagnetization rates in GSFEJs after gate tuning (black) compared to bare TiO<sub>x</sub>|Co (gray). (d)  $\tau_m$  as a function of normalized contact conductance  $G_j$  for each thickness.

The minor asymmetry in  $\tau_m$  about  $\Delta V$  can propagate from the asymmetry in  $R_j$  for electron-hole doping regimes and an uneven junction spin dependence, leading to asymmetry in electron-hole spin injection [27]. Compared to the slowest  $\tau_m$  (maximum  $\tau_m$  at  $V_G = V_D$ ), the junctions with the oxide barrier display a significant decrease in  $\tau_m$  up to 29%, 46%, and 39% for 10, 20, and 30 nm Co thickness, respectively. For the sample without TiO<sub>x</sub> and 30 nm Co, a maximum decrease of 41% is obtained. Strikingly, compared to bare cobalt films (Table S1 in SM [16]), as shown in Fig. 3(c), the demagnetization speed effectively doubles for gate-tuned GSFEJs as  $\tau_{\text{FM}}/\tau_{\text{Gr|FM}}^{\text{min}} > 2$ . Thus, by applying gate voltage and tuning the carrier density to  $\sim 10^{11}$ – $10^{12}$  cm<sup>-2</sup> in graphene, more than 100% faster demagnetization rates can be achieved in GSFEJs. Notably, for all our heterostructures, a substantial reduction in  $\tau_m$  (with the lowest  $\tau_m \approx 93$  fs) is observed in both electron and hole conduction regimes as the carrier concentration in graphene is tuned. The ability to significantly control demagnetization through gate-tunable field-effect junctions represents a major advancement.

To support our experimental results, we performed numerical simulations based on the superdiffusive transport theory [7] to model the magnetization quenching in Co.

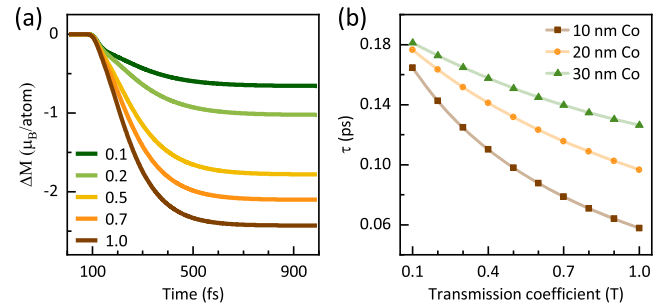


FIG. 4. Superdiffusive spin transport simulations. (a) Simulated magnetization decay for varying transmission coefficients ( $T$ ) in 30 nm Co. (b)  $\tau$  versus  $T$  for Co thicknesses of 10, 20, and 30 nm.

Details of the model, including parameter descriptions and the governing equations, are provided in Appendix B. The results of these simulations are illustrated in Fig. 4(a), where we display  $\Delta M$  in the ferromagnetic layer of 30-nm-thick Co for different interface transmission coefficients ( $T$ ). While  $T$  does not explicitly appear in Eq. (B1), it is accounted for through the dynamic electron flux term. As the transmission coefficient increases, we observe a corresponding faster decay.

Figure 4(b) shows the simulated results for three Co layers of 10, 20, and 30 nm, respectively, with varying  $T$ , to simulate the effect of the change in the gate voltage on the graphene layer. We observe that for higher  $T$  (i.e., higher injection into the graphene layer),  $\tau$  is significantly reduced. The  $\tau$  at low  $T$  is about 40%–180% larger than for high  $T$ , depending on the layer thickness. Thus, the demagnetization rate increases for higher transmission, corresponding to a faster injection of spin currents flowing into graphene. Such a trend is partially observed in experiments, where thinner Co layers demagnetize faster [Fig. 2(b)], with deviations in the thickness dependence for thicker samples and gate-dependent enhancements [Fig. 3(b)]. The experimentally obtained  $\tau_m$  values vary less with Co thickness than the calculated ones. These differences can be attributed to extrinsic scattering caused by inhomogeneities, roughness, grain boundaries, and charge transfer doping in graphene. In addition, for higher thickness ( $t > \lambda_s$  and  $\lambda_p$ ), the density of electrons injected into the graphene layer varies, and the transmission effect on the  $\tau_m$  becomes less relevant. Additionally, the observed differences can play out in the experimental error bars resulting from time resolution and sample preparation. Despite these factors, our simulations unambiguously reveal that the electric field tuning of  $T$  is an efficient method for controlling interface spin transport and magnetization dynamics for all thicknesses. It is worth noting that this mechanism is distinct from other interfacial effects like resonant precession-induced spin pumping, which are specific to a particular FM thickness, lead to transverse spin injection, and usually dominate at lower thicknesses [28]. Considering that conductance varies as transmission, comparing Figs. 3(d)

and 4(b), we can observe an evident correlation, with nearly or more than 100% enhancement in  $1/\tau$  as the conductance or transmission values are increased. Although we cannot entirely rule out spin-flip scattering events at the Gr|FM boundary, to the extent that the transmission dependence of the  $\tau_m$  is concerned, the superdiffusion of laser-excited electrons across the Gr|FM junction can satisfactorily explain our observed gate-controlled spin dynamics within a quantitative order of magnitude. Electrostatic gating directly tunes the longitudinal spin current transmission across the Gr|FM interface. Applying gate voltage away from  $V_D$  linearly increases the carrier density in graphene, thereby shifting its Fermi level, reducing the junction  $R_J$ , and consequently enhancing the transmission coefficient  $T$  ( $\propto G_J$ ). In the superdiffusive spin transport model, a larger  $T$  facilitates more efficient drainage of spin angular momentum from Co, leading to a reduction in  $\tau_m$ . This mechanistic picture is directly demonstrated in our spin-field-effect junctions: gate-induced enhanced  $G_J$  results in faster  $\tau_m$ , a trend reproduced by our simulations (Fig. 4). This understanding enables a new class of devices where spin dynamics can be dynamically modulated through gate control, without altering material composition or geometry.

The femtosecond laser-induced demagnetization phenomenon in FMs [29] has been widely discussed in terms of Elliott-Yafet and similar spin-flip scattering processes, such as the cooperative effect of intrinsic spin-orbit coupling and the laser field [30], local magnon-mediated spin-flip scattering [31], Coulomb exchange [32], impurity centers or phonons [33], and relativistic electron-phonon interactions [34]. On the other hand, the superdiffusive spin transport theory [7] explains how longitudinal spin-dependent transport of hot electrons to the adjacent conducting layer can account for rapid magnetization quenching [35], even in the absence of direct laser absorption by the FM, as seen in the indirect demagnetization of Ni by hot electrons generated in an adjacent Au layer [5]. Similarly, in Ni/Ru/Fe trilayer structures, the demagnetization of a Ni layer enhances transient magnetization in Fe, attributed to spin currents generated upon laser excitation [6]. Heterostructures of FMs with graphene have been seen to give rise to proximity-induced magnetic interactions [36–38] and are promising for subpicosecond magnetization decay [39,40]. The field-tunable spin currents demonstrated in GSFEJs enable faster demagnetization, establishing a new functional pathway for high-speed graphene spintronics. By electric-field-tuned Gr|FM junction conductance, our experiments directly corroborate the predictions of superdiffusive spin transport theory. This is a significant development because the carrier density in graphene can be increased to very high values beyond  $10^{14}$  cm<sup>-2</sup>, reaching van Hove singularities [41] for further reduction in  $\tau_m$  approaching predictions of a few femtoseconds [30]. Thus, the GSFEJ provides a framework for a whole new set of investigations to directly validate and explore ultrafast spin transport and spin injection in

semiconducting 2D materials such as MoS<sub>2</sub>, MoSe<sub>2</sub>, and WSe<sub>2</sub>, as well as 2D magnetic materials like CrI<sub>3</sub>, and their electrically tunable van der Waals spinterfaces [9]. Exploration of this domain is of key significance for precision spin current sensors, spin memory and logic operations with lower energy-delay products, which are vital for handling data-intensive tasks. It could enable components with greater longevity [42], reduced latency, and faster data speeds for magnetoresistive random-access memory and gate-based spintronic compute-in-memory architectures [43], with potential for hot-carrier accelerated subnanosecond operations [44]. In addition, due to graphene's high thermal conductivity and better heat management, CVD graphene is promising for the scalability of GSFEJs.

In summary, we have demonstrated gate-tunable ultrafast spin currents and dynamics in graphene spin-field-effect junctions, achieving more than a 100% enhancement in demagnetization rate. These results establish electrical control over superdiffusive spin transport and ultrafast spin injection into 2D quantum materials, offering new opportunities for tunable femtosecond spin dynamics experiments. The demonstrated mechanism enables dynamic control of spin angular momentum flow, with implications for scalable spin-logic, quantum sensing, and next-generation THz spintronic technologies.

*Acknowledgments*—We gratefully acknowledge funding from the European Research Council (ERC) Project SPINNER (Grant No. 101002772), Stiftelsen Olle Engkvist Byggmästare (Grant No. 200–0602), the Swedish Research Council VR (Grants No. 2021-05932 and No. 2024-05531), and the Knut and Alice Wallenberg Foundation (Grants No. 2022.0079 and No. 2023.0336). Numerical calculations were enabled by resources from the National Academic Infrastructure for Supercomputing in Sweden (NAISS) at NSC Linköping, partially funded by VR through Grant Agreement No. 2022-06725. A. B. gratefully acknowledges financial assistance from the S. N. Bose National Centre for Basic Sciences (SNBNCBS), India (Project No. SNB/AB/11-12/96) and the Department of Science and Technology (DST), Government of India (Grant No. DST/NM/TUE/QM-3/2019-1C-SNB). S. M. acknowledges DST, India, for financial support from the INSPIRE fellowship. D. M. and M. V. K. thank H. Nameirakpam and G. Datt for helpful assistance.

*Data availability*—The data that support the findings of this Letter are not publicly available. The data are available from the authors upon reasonable request.

- 
- [1] H. Dery, P. Dalal, Ł. Cywiński, and L. J. Sham, Spin-based logic in semiconductors for reconfigurable large-scale circuits, *Nature (London)* **447**, 573 (2007).
  - [2] J. Torrey et al., Neuromorphic computing with nanoscale spintronic oscillators, *Nature (London)* **547**, 428 (2017).

- [3] C. L. Degen, F. Reinhard, and P. Cappellaro, Quantum sensing, *Rev. Mod. Phys.* **89**, 035002 (2017).
- [4] T. Kampfrath *et al.*, Terahertz spin current pulses controlled by magnetic heterostructures, *Nat. Nanotechnol.* **8**, 256 (2013).
- [5] A. Eschenlohr, M. Battiato, P. Maldonado, N. Pontius, T. Kachel, K. Hollmack, R. Mitzner, A. Föhlisch, P. M. Oppeneer, and C. Stamm, Ultrafast spin transport as key to femtosecond demagnetization, *Nat. Mater.* **12**, 332 (2013).
- [6] D. Rudolf *et al.*, Ultrafast magnetization enhancement in metallic multilayers driven by superdiffusive spin current, *Nat. Commun.* **3**, 1036 (2012).
- [7] M. Battiato, K. Carva, and P. M. Oppeneer, Superdiffusive spin transport as a mechanism of ultrafast demagnetization, *Phys. Rev. Lett.* **105**, 027203 (2010).
- [8] A. Fert and H. Jaffrès, Conditions for efficient spin injection from a ferromagnetic metal into a semiconductor, *Phys. Rev. B* **64**, 184420 (2001).
- [9] J. F. Dayen, S. J. Ray, O. Karis, I. J. Vera-Marun, and M. V. Kamalakar, Two-dimensional van der Waals spinterfaces and magnetic-interfaces, *Appl. Phys. Rev.* **7**, 011303 (2020).
- [10] A. H. Castro Neto, F. Guinea, N. M. R. Peres, K. S. Novoselov, and A. K. Geim, The electronic properties of graphene, *Rev. Mod. Phys.* **81**, 109 (2009).
- [11] A. S. Mayorov *et al.*, Micrometer-scale ballistic transport in encapsulated graphene at room temperature, *Nano Lett.* **11**, 2396 (2011).
- [12] D. Huertas-Hernando, F. Guinea, and A. Brataas, Spin-orbit-mediated spin relaxation in graphene, *Phys. Rev. Lett.* **103**, 146801 (2009).
- [13] J. Panda, M. Ramu, O. Karis, T. Sarkar, and M. V. Kamalakar, Ultimate spin currents in commercial chemical vapor deposited graphene, *ACS Nano* **14**, 12771 (2020).
- [14] N. Tombros, C. Jozsa, M. Popinciuc, H. T. Jonkman, and B. J. Van Wees, Electronic spin transport and spin precession in single graphene layers at room temperature, *Nature (London)* **448**, 571 (2007).
- [15] A. Avsar, H. Ochoa, F. Guinea, B. Özyilmaz, B. J. van Wees, and I. J. Vera-Marun, Colloquium: Spintronics in graphene and other two-dimensional materials, *Rev. Mod. Phys.* **92**, 021003 (2020).
- [16] See Supplemental Material at <http://link.aps.org/supplemental/10.1103/7ldk-csp9> for details on static and time-resolved magneto-optical Kerr effect (MOKE) characterizations, computational methods for superdiffusive spin transport, and supporting figures and tables, which includes Refs. [17–22].
- [17] A. J. Berger, W. Amamou, S. P. White, R. Adur, Y. Pu, R. K. Kawakami, and P. C. Hammel, Magnetization dynamics of cobalt grown on graphene, *J. Appl. Phys.* **115**, 17C510 (2014).
- [18] A. Barman and J. Sinha, *Spin Dynamics and Damping in Ferromagnetic Thin Films and Nanostructures* (Springer International Publishing AG, Cham, 2018).
- [19] J. Wiczorek, A. Eschenlohr, B. Weidtmann, M. Rösner, N. Berggard, A. Tarasevitch, T. O. Wehling, and U. Bovensiepen, Separation of ultrafast spin currents and spin-flip scattering in Co/Cu(001) driven by femtosecond laser excitation employing the complex magneto-optical Kerr effect, *Phys. Rev. B* **92**, 174410 (2015).
- [20] T. H. Dang *et al.*, Ultrafast spin-currents and charge conversion at 3d-5d interfaces probed by time-domain terahertz spectroscopy, *Appl. Phys. Rev.* **7**, 041409 (2020).
- [21] I. A. Nechaev and E. V. Chulkov, Quasiparticle dynamics in ferromagnetic compounds of the Co-Fe and Ni-Fe systems, *Eur. Phys. J. B* **77**, 31 (2010).
- [22] W. M. Haynes, *CRC Handbook of Chemistry and Physics*, 97th ed. (CRC Press, Boca Raton, 2016).
- [23] J. Bass and W. P. Pratt, Spin-diffusion lengths in metals and alloys, and spin-flipping at metal/metal interfaces: An experimentalist's critical review, *J. Phys. Condens. Matter* **19**, 183201 (2007).
- [24] D. Belotcerkovtceva, R. P. Maciel, E. Berggren, R. Maddu, T. Sarkar, Y. O. Kvashnin, D. Thonig, A. Lindblad, O. Eriksson, and M. V. Kamalakar, Insights and implications of intricate surface charge transfer and  $sp^3$ -defects in graphene/metal oxide interfaces, *ACS Appl. Mater. Interfaces* **14**, 36209 (2022).
- [25] I. G. Serrano, J. Panda, F. Denoel, Ö. Vallin, D. Phuyal, O. Karis, and M. V. Kamalakar, Two-dimensional flexible high diffusive spin circuits, *Nano Lett.* **19**, 666 (2019).
- [26] M. V. Kamalakar, C. Groenveld, A. Dankert, and S. P. Dash, Long distance spin communication in chemical vapour deposited graphene, *Nat. Commun.* **6**, 6766 (2015).
- [27] W. Han, W. H. Wang, K. Pi, K. M. McCreary, W. Bao, Y. Li, F. Miao, C. N. Lau, and R. K. Kawakami, Electron-hole asymmetry of spin injection and transport in single-layer graphene, *Phys. Rev. Lett.* **102**, 137205 (2009).
- [28] Y. Tserkovnyak, A. Brataas, and G. E. W. Bauer, Enhanced Gilbert damping in thin ferromagnetic films, *Phys. Rev. Lett.* **88**, 117601 (2002).
- [29] E. Beaupaire, J.-C. Merle, A. Daunois, and J.-Y. Bigot, Ultrafast spin dynamics in ferromagnetic nickel, *Phys. Rev. Lett.* **76**, 4250 (1996).
- [30] G. P. Zhang and W. Hübner, Laser-induced ultrafast demagnetization in ferromagnetic metals, *Phys. Rev. Lett.* **85**, 3025 (2000).
- [31] E. Carpene, E. Mancini, C. Dallera, M. Brenna, E. Puppini, and S. De Silvestri, Dynamics of electron-magnon interaction and ultrafast demagnetization in thin iron films, *Phys. Rev. B* **78**, 174422 (2008).
- [32] M. Krauß, T. Roth, S. Alebrand, D. Steil, M. Cinchetti, M. Aeschlimann, and H. C. Schneider, Ultrafast demagnetization of ferromagnetic transition metals: The role of the Coulomb interaction, *Phys. Rev. B* **80**, 180407(R) (2009).
- [33] J. Y. Bigot, M. Vomir, and E. Beaupaire, Coherent ultrafast magnetism induced by femtosecond laser pulses, *Nat. Phys.* **5**, 515 (2009).
- [34] B. Koopmans, G. Malinowski, F. Dalla Longa, D. Steiauf, M. Fähnle, T. Roth, M. Cinchetti, and M. Aeschlimann, Explaining the paradoxical diversity of ultrafast laser-induced demagnetization, *Nat. Mater.* **9**, 259 (2010).
- [35] M. Hofherr *et al.*, Speed and efficiency of femtosecond spin current injection into a nonmagnetic material, *Phys. Rev. B* **96**, 100403(R) (2017).
- [36] F. Ajejas *et al.*, Unraveling Dzyaloshinskii-Moriya interaction and chiral nature of graphene/cobalt interface, *Nano Lett.* **18**, 5364 (2018).

- [37] A. K. Chaurasiya, A. Kumar, R. Gupta, S. Chaudhary, P. K. Muduli, and A. Barman, Direct observation of unusual interfacial Dzyaloshinskii-Moriya interaction in graphene/NiFe/Ta heterostructures, *Phys. Rev. B* **99**, 035402 (2019).
- [38] H. C. Mertins *et al.*, Giant magneto-optical Faraday effect of graphene on Co in the soft x-ray range, *Phys. Rev. B* **98**, 064408 (2018).
- [39] S. N. Panda, S. Majumder, S. Choudhury, A. Bhattacharya, S. Sinha, and A. Barman, Femtosecond laser-induced spin dynamics in single-layer graphene/CoFeB thin films, *Nanoscale* **13**, 13709 (2021).
- [40] S. Mondal, Y. Lin, D. Polley, C. Su, A. Zettl, S. Salahuddin, and J. Bokor, Accelerated ultrafast magnetization dynamics at graphene/CoGd interfaces, *ACS Nano* **16**, 9620 (2022).
- [41] P. Rosenzweig, H. Karakachian, D. Marchenko, K. Küster, and U. Starke, Overdoping graphene beyond the van Hove singularity, *Phys. Rev. Lett.* **125**, 176403 (2020).
- [42] B. Dieny *et al.*, Opportunities and challenges for spintronics in the microelectronics industry, *Nat. Electron.* **3**, 446 (2020).
- [43] Y. C. Chiu *et al.*, A CMOS-integrated spintronic compute-in-memory macro for secure AI edge devices, *Nat. Electron.* **6**, 534 (2023).
- [44] Y. Xiang, C. Wang, C. Liu, T. Wang, Y. Jiang, Y. Wang, S. Wang, and P. Zhou, Subnanosecond flash memory enabled by 2D-enhanced hot-carrier injection, *Nature (London)* **641**, 90 (2025).
- [45] F. Dalla Longa, J. T. Kohlhepp, W. J. M. De Jonge, and B. Koopmans, Influence of photon angular momentum on ultrafast demagnetization in nickel, *Phys. Rev. B* **75**, 224431 (2007).
- [46] G. Malinowski, F. Dalla Longa, J. H. H. Rietjens, P. V. Paluskar, R. Huijink, H. J. M. Swagten, and B. Koopmans, Control of speed and efficiency of ultrafast demagnetization by direct transfer of spin angular momentum, *Nat. Phys.* **4**, 855 (2008).
- [47] M. Battiato, K. Carva, and P. M. Oppeneer, Theory of laser-induced ultrafast superdiffusive spin transport in layered heterostructures, *Phys. Rev. B* **86**, 024404 (2012).
- [48] W. T. Lu, Y. Zhao, M. Battiato, Y. Wu, and Z. Yuan, Interface reflectivity of a superdiffusive spin current in ultrafast demagnetization and terahertz emission, *Phys. Rev. B* **101**, 014435 (2020).

## End Matter

*Appendix A: Three-temperature thermodynamic model*—We analyze the TR-MOKE curves with the phenomenological three-temperature thermodynamic model, wherein the dynamics of demagnetization and fast relaxation are expressed as follows [45,46]:

$$-\frac{\Delta M_z}{M_z} = \left[ \left\{ \frac{A_1}{\sqrt{\frac{t}{\tau_0} + 1}} + \frac{A_1 \tau_m - A_2 \tau_e}{\tau_e - \tau_m} e^{-\frac{t}{\tau_m}} + \frac{A_2 \tau_e - A_1 \tau_e}{\tau_e - \tau_m} e^{-\frac{t}{\tau_e}} \right\} \times H(t) + A_3 \delta(t) \right] \otimes G(t), \quad (\text{A1})$$

where  $A_1$  is the normalized magnetization amplitude at the end of the fast remagnetization process, indicating re-equilibration between the electron, lattice, and spin systems.  $A_2$  scales with the initial electron-temperature rise and hence the maximum magnetization quenching, while  $A_3$  quantifies the state-filling effect at the onset of demagnetization.  $H(t)$  denotes the Heaviside step function,  $\delta(t)$  is the Dirac delta function, and  $G(t)$  represents the Gaussian laser pulse. The cooling time by heat diffusion is described by  $\tau_0$ . According to this model, when a femtosecond laser pulse strikes the device, the electron temperature increases, generating hot electrons that excite the spin subsystem [29]. Excitation of the spin subsystem leads to a quenching of the macroscopic magnetization in approximately the first few hundred femtoseconds, known as ultrafast demagnetization, where the demagnetization time is denoted by  $\tau_m$ . Subsequently, the quenched magnetization relaxes to its original equilibrium state due to the energy rebalancing between the

electron, spin, and lattice subsystems over two distinct timescales. The first corresponds to the fast remagnetization process with a characteristic time  $\tau_e$ . Finally, slow remagnetization occurs due to the energy dissipation from the lattice bath of the magnetic layer to the substrate or graphene. This phenomenological description with characteristic times provides an established method of characterizing femtosecond laser-induced demagnetization processes in FMs.

*Appendix B: Superdiffusive transport model and simulation parameters*—The superdiffusive spin transport theory derives its name from the distinct transport mechanism. On an fs timescale, laser-excited electrons undergo a few scatterings, reducing their mobility and placing them between ballistic and diffusive transport. The higher mobility of the outward-diffusing laser-excited majority spins directly leads to the longitudinal quenching of the magnetization of the FM in the excitation region. The different lifetimes of the superdiffusive electron spins in different materials make the spin dynamics ( $\tau_m$  and  $\tau_e$ ) dependent on the boundary between the FM and the adjacent material, in our case, graphene and  $\text{TiO}_x$ .

In the framework of this theory, we attribute the different demagnetization dynamics that we observed upon the electric-field-tuned conductance of the graphene layer to the spin transport at the boundary in the heterostructure. The model is a quasi-1D differential equation for the density  $n_\sigma(\epsilon, z, t)$  of excited electrons with spin  $\sigma$ , energy  $\epsilon$ , and space and time coordinates ( $z, t$ ), given by

equation (B1),

$$\frac{\partial n_\sigma}{\partial t} + \frac{n_\sigma}{\tau_\sigma} = \left( -\frac{\partial}{\partial z} \hat{\phi} + \hat{I} \right) S_\sigma^{\text{eff}}. \quad (\text{B1})$$

For the sake of simplicity, we omitted the energy, position, and time dependence from Eq. (B1) (details on the derivation of the equation are reported in Refs. [7,47].) The quantity  $\tau_\sigma$  is an energy-dependent quantity that represents the lifetime of excited electrons, i.e., the time between two scattering events,  $\hat{\phi}$  is the flux operator accounting for the dynamics of the electrons in the material,

such as electron scattering, spin-flip, and boundary scattering events.  $\hat{I}$  is the identity operator, while  $S_\sigma^{\text{eff}}$  is the effective spin source, which is composed of the laser-excited electrons  $S^{\text{ext}}$  modeled as a Gaussian pulse, and the electrons excited from scattering events  $S^p$ , so that  $S^{\text{eff}} = S^{\text{ext}} + S^p$ . The longitudinal spin current derived from the solution of Eq. (B1) quantitatively connects with the magnetization quenching ( $\Delta M$ ) in the excited layer [7,47,48]. Relevant details on the electron excitation profiles, penetration depth, and parameter derivations used in our simulations can be found in Refs. [19–22].